The evolution of the Sun's birth cluster and the search for the solar siblings with *Gaia*

C. A. Martínez-Barbosa,[1]⋆ A. G. A. Brown,[1]⋆ T. Boekholt,[1] S. Portegies Zwart,[1] E. Antiche[2] and T. Antoja[3]

[1]*Leiden Observatory, Leiden University, P.B. 9513, Leiden NL-2300 RA, the Netherlands*
[2]*Departament d' Astronomia i Meteorologia, Universitat de Barcelona, Institut de Ciències del Cosmos, IEEC, Martí Franquès 1, E-08028 Barcelona, Spain*
[3]*Scientific Support Office, Directorate of Science and Robotic Exploration, European Space Research and Technology Centre (ESA/ESTEC), Keplerlaan 1, Noordwijk NL-2201 AZ, the Netherlands*

ABSTRACT

We use self-consistent numerical simulations of the evolution and disruption of the Sun's birth cluster in the Milky Way potential to investigate the present-day phase-space distribution of the Sun's siblings. The simulations include the gravitational *N*-body forces within the cluster and the effects of stellar evolution on the cluster population. In addition, the gravitational forces due to the Milky Way potential are accounted for in a self-consistent manner. Our aim is to understand how the astrometric and radial velocity data from the *Gaia* mission can be used to pre-select solar sibling candidates. We vary the initial conditions of the Sun's birth cluster, as well as the parameters of the Galactic potential. In particular, we use different configurations and strengths of the bar and spiral arms. We show that the disruption time-scales of the cluster are insensitive to the details of the non-axisymmetric components of the Milky Way model and we make predictions, averaged over the different simulated possibilities, about the number of solar siblings that should appear in surveys such as *Gaia* or GALAH. We find a large variety of present-day phase-space distributions of solar siblings, which depend on the cluster initial conditions and the Milky Way model parameters. We show that nevertheless robust predictions can be made about the location of the solar siblings in the space of parallaxes (ϖ), proper motions (μ) and radial velocities (V_r). By calculating the ratio of the number of simulated solar siblings to that of the number of stars in a model Galactic disc, we find that this ratio is above 0.5 in the region given by: $\varpi \geq 5$ mas, $4 \leq \mu \leq 6$ mas yr^{-1}, and $-2 \leq V_r \leq 0$ km s^{-1}. Selecting stars from this region should increase the probability of success in identifying solar siblings through follow-up observations. However the proposed pre-selection criterion is sensitive to our assumptions, in particular about the Galactic potential. Using a more realistic potential (e.g. including transient spiral structure and molecular clouds) would make the pre-selection of solar sibling candidates based on astrometric and radial velocity data very inefficient. This reinforces the need for large-scale surveys to determine precise astrophysical properties of stars, in particular their ages and chemical abundances, if we want to identify the solar family.

Key words: Sun: general – Galaxy: kinematics and dynamics – open clusters and associations: general – solar neighbourhood.

1 INTRODUCTION

Since most of the stars are born in star clusters (Lada & Lada 2003), these systems are considered the building blocks of galaxies. In the Milky Way, star clusters located in the Galactic halo (Globular clusters) populate the Galactic disc through mergers (Lee et al. 2013). On the other hand, star clusters formed in the Galactic disc (open clusters) supply new stars to the disc of the Galaxy through several processes, such as shocks from encounters with spiral arms and giant molecular clouds (Gieles et al. 2006; Gieles, Athanassoula & Portegies Zwart 2007).

The dynamical evolution of star clusters involves several physical mechanisms. At earlier stages of their evolution, star clusters lose mass mainly due to stellar evolution and two-body

⋆ E-mail: cmartinez@strw.leidenuniv.nl (CAM-B); brown@strw.leidenuniv.nl (AGAB)

relaxation processes, which in turn, enlarge the size of star clusters (Takahashi & Portegies Zwart 2000; Baumgardt & Makino 2003; Madrid, Hurley & Sippel 2012). This evolutionary stage is called the expansion phase (Gieles, Heggie & Zhao 2011), which takes about 40% of the star cluster's lifetime. Once star clusters overcome the expansion phase, the effects of the external tidal field of the Galaxy become important, depending on their location with respect to the Galactic Centre. This stage is called the evaporation phase (Gieles et al. 2011) and it is characterized by the gradual dissolution of star clusters in the Galaxy.

The dissolution rate of star clusters depends on their Galacto-centric distance (Madrid et al. 2012), orbit (Baumgardt & Makino 2003), orbital inclination (Webb et al. 2014) and on Galaxy properties, such as the mass and size of the Galactic disc (Madrid, Hurley & Martig 2014). Additionally, open clusters in the Milky Way are also dissolved due to non-axisymmetric perturbations such as bars (Berentzen & Athanassoula 2012), spiral arms (Gieles et al. 2007) and giant molecular clouds (Gieles et al. 2006; Lamers & Gieles 2006). The strongest tidal stripping occurs at times when open clusters cross regions of high-density gas, for instance, during spiral arms passages (Gieles et al. 2007; Kruijssen et al. 2011) or during collisions with giant molecular clouds (Gieles et al. 2006). Open clusters can also radially migrate over distances of up to 1 kpc in a short time-scale (∼100 Myr) when the Galactic spiral structure is transient (Fujii & Baba 2012). This radial migration process can also be efficient in the absence of transient structure if the resonances due the bar and spiral structure overlap (Minchev & Famaey 2010). Radial migration affects the orbits of open clusters in the Galaxy, increasing or decreasing their perigalacticon distance, which in turn influences their dissolution times (see e.g. Jílková et al. 2012).

The high eccentricities and inclinations observed in the Edgeworth–Kuiper belt objects together with the discovery of decay products of ^{60}Fe and other radioactive elements in the meteorite fossil record, suggest that the Sun was born in an open cluster 4.6 Gyr ago (Portegies Zwart 2009, and references therein). Identifying the stars that were formed together with the Sun (the solar siblings) would enable the determination of the Galactic birth radius of the Sun as well as further constrain the properties of its birth cluster (Adams 2010; Bland-Hawthorn, Krumholz & Freeman 2010). The birth radius affects the evolution of the Solar system, and in particular the Oort cloud, which is sensitive to the Galactic environment the Sun passes through along its orbit (e.g. Portegies Zwart & Jílková 2015).

The Sun's birth cluster will undergo all the disruptive processes described above and thus dissolve, leading to the spreading out of its stars over the Galactic disc. The subsequent distribution of the solar siblings was studied by Portegies Zwart (2009), who evolved the Sun's birth cluster in an axisymmetric model for the Galactic potential and concluded that tens of solar siblings might still be present within a distance of 100 pc from the Sun. Several attempts have since been made to find solar siblings (e.g. Brown, Portegies Zwart & Bean 2010; Bobylev et al. 2011; Liu et al. 2015); however, only four plausible candidates have been identified so far (Batista & Fernandes 2012; Batista et al. 2014; Ramírez et al. 2014). This small number of observed solar siblings might be a consequence of the lack of accurate predictions of the present-day phase-space distribution of solar siblings together with insufficiently accurate stellar kinematic data.

Brown et al. (2010) used test particle simulations to predict the current distribution of solar siblings in the Milky Way. They concluded that stars with parallaxes (ϖ) ≥10 mas and proper motions (μ) ≤6.5 mas yr^{-1}, should be considered solar sibling candidates.

Their conclusions were criticized by Mishurov & Acharova (2011) who pointed out that in more realistic Galactic potentials, the solar siblings are expected to be much more spread out over the Galactic disc. For small birth clusters (few thousand stars with a total mass of the order of 1000 M$_\odot$), such as employed by Brown et al. (2010) and Portegies Zwart (2009), Mishurov & Acharova (2011) predict that practically no solar siblings will currently be located within 100 pc from the Sun. However, for larger birth clusters (of the order of 10^4 stars, in line with predictions from e.g. Dukes & Krumholz 2012) one can still expect to find a good number of siblings presently orbiting the Galaxy within 100 pc from the Sun.

Ongoing surveys of our galaxy, in particular the *Gaia* mission (Lindegren et al. 2008) and the GALAH survey (GALactic Archeology with Hermes, De Silva et al. 2015), will provide large samples of stars with accurately determined distances, space motions, and chemical abundance patterns, thus enabling a much improved search for the Sun's siblings. In this paper, we investigate the potential of the *Gaia* astrometric and radial velocity data to narrow down the selection of candidate solar siblings for which detailed chemical abundance studies should be undertaken in order to identify the true siblings. Our investigation is done by performing simulations of the evolution and disruption of the Sun's birth cluster in a realistic (although static) Galactic potential, including the bar and spiral arms. The aim is to predict the present-day phase-space distribution of the siblings and simulate the astrometric and radial velocity data collected by *Gaia*. We include the internal *N*-body processes in the cluster to account for the disruption time-scale. We use a full stellar mass spectrum and a parametrized stellar evolution code to make accurate predictions of how the solar siblings are observed by *Gaia*. To this end, we also account for the effects of extinction and reddening.

The rest of this paper is organized as follows. In Section 2, we describe the simulations. In Section 3, we explore the evolution and disruption of the Sun's birth cluster due to the bar and spiral arms of the Galaxy. In Section 4, we present the current phase-space distribution of solar siblings obtained from the simulations. In Section 5, we make use of the simulated positions and motions of the solar siblings to investigate the robustness of the selection criterion proposed by Brown et al. (2010) to the uncertainties in the present-day phase-space distribution of the solar siblings. An updated set of selection criteria based on parallax, proper motion and radial velocity information is presented. In Section 6, we use these criteria to examine stars that were previously suggested as solar siblings candidates and further discuss our results. In Section 7, we summarize.

2 SIMULATION SET-UP

The goals of the simulations of the Sun's birth cluster are to predict the present-day phase-space distribution of the solar siblings and how these are expected to appear in the *Gaia* catalogue. In particular, we wish to account for the uncertainties in the initial conditions of the birth cluster and the parameters of the Milky Way potential. The predictions of the *Gaia* observations require the use of a realistic mass spectrum for the siblings, and accounting for stellar evolution and extinction and interstellar reddening effects. We thus employ the following elements in the simulations.

Galactic model: the Milky Way potential is described by an analytic model containing a disc, bulge and halo, as well as a bar and spiral arms. The parameters of the bar and spiral arms are varied

Table 1. Parameters of the Milky Way model potential.

Axisymmetric component	
Mass of the bulge (M_b)	1.41×10^{10} M$_\odot$
Scale length bulge (b_1)	0.38 kpc
Disc mass (M_d)	8.56×10^{10} M$_\odot$
Scale length disc 1 (a_2)	5.31 kpc
Scale length disc 2 (b_2)	0.25 kpc
Scale length (M_h)	1.07×10^{11} M$_\odot$
Scale length halo (a_3)	12 kpc
Central bar	
Pattern speed (Ω_{bar})	40–70 km s^{-1} kpc^{-1}
Semi-major axis (a)	3.12 kpc
Axis ratio (b/a)	0.37
Mass (M_{bar})	9.8×10^9–1.4×10^{10} M$_\odot$
Present-day orientation	20°
Initial orientation	1°–167°
Spiral arms	
Pattern speed (Ω_{sp})	15–30 km s^{-1} kpc^{-1}
Locus beginning (R_{sp})	3.12 kpc
Number of spiral arms (m)	2, 4
Spiral amplitude (A_{sp})	650–1100 km^2 s^{-2} kpc^{-1}
Pitch angle (i)	12°.8
Scale length (R_Σ)	2.5 kpc
Present-day orientation	20°
Initial orientation	103°–173°

in the simulations to account for uncertainties in their strengths and pattern speeds (Section 2.1).

Cluster model: the Sun's birth cluster is modelled with a mass spectrum for the stars and we account for the gravitational *N*-body effects within the cluster as well as the effect of the Galaxy's gravitational field on the cluster stars. The use of *N*-body models for the birth cluster is motivated by the desire to account for the disruption time of the cluster which can be a substantial fraction of the lifetime of the Sun (Section 2.2).

Stellar evolution: predicting the observations of the Sun's birth cluster by *Gaia* requires that we account for the mass-dependent evolution of the solar siblings, in order to obtain the correct present-day apparent magnitudes and colours which are used to predict which stars end up in the *Gaia* catalogue. This prediction also requires us to account for interstellar extinction and reddening for which we employ a Galactic extinction model (Sections 2.3 and 5).

These elements are described in more detail in the subsequent subsections.

2.1 Galactic model

We use an analytical potential to model the Milky Way. This potential contains two parts: an axisymmetric component, which corresponds to a bulge, disc and a dark matter halo, and a non-axisymmetric component which includes a central bar and spiral arms. Below we explain these components in more detail.

Axisymmetric component: we use the potential of Allen & Santillán (1991) to model the axisymmetric component of the Galaxy. In this approach, the bulge is modelled with a Plummer (Plummer 1911) potential; the disc is modelled with a Miyamoto–Nagai (Miyamoto & Nagai 1975) potential and the dark matter halo with a logarithmic potential. The parameters used to model the axisymmetric component of the Galaxy are listed in Table 1.

The model introduced by Allen & Santillán (1991) predicts a rotational velocity of 220 kms^{-1} at the solar radius, which

does not match with the recent observational estimates (see e.g McMillan 2011; Reid et al. 2014). However, Jílková et al. (2012) did not find substantial variations in the orbits of open clusters when using different models of the axisymmetric structure of the Galaxy. Therefore, we do not expect that the evolution of the Sun's birth cluster and the present-day distribution of solar siblings will be affected due to the choice of the axisymmetric potential model.

The Galactic bar: the central bar is modelled with a Ferrers potential (Ferrers 1877) which describes the potential associated with an elliptical distribution of mass. In an inertial frame located at the Galactic Centre, the bar rotates with a constant pattern speed of 40–70 kms^{-1}kpc^{-1} (Martínez-Barbosa, Brown & Portegies Zwart 2015). This range of angular velocities places the Outer Lindblad resonance of the bar (OLR$_{bar}$) at 10–5 kpc from the Galactic Centre. In the same inertial frame, the present-day orientation of the bar with respect to the negative *x*-axis is 20° (Pichardo, Martos & Moreno 2004; Romero-Gómez et al. 2011; Pichardo et al. 2012, and references therein). In the left-hand panel of Fig. 1, we show the present-day orientation of the Galactic bar. In Table 1, we show the parameters used in this study. For further details on the choice of the bar parameters, we refer the reader to Martínez-Barbosa et al. (2015).

The spiral arms: we model the spiral arms as periodic perturbations of the axisymmetric potential (tight winding approximation; Lin, Yuan & Shu 1969). The spiral arms rotate with a constant pattern speed of 15–30 kms^{-1}kpc^{-1} (Martínez-Barbosa et al. 2015). This range of values places the co-rotation resonance of these structures (CR$_{sp}$) at 14–7 kpc from the Galactic Centre. We assume that the Galaxy has two or four non-transient spiral arms with the same amplitude. A schematic picture of the present-day configuration of the spiral arms is shown in the left-hand and middle panels of Fig. 1. The parameters of the spiral arms used in this study are listed in Table 1. For further details on the choice of these parameters, we refer the reader to Martínez-Barbosa et al. (2015).

Initial orientation of the bar and spiral arms: the orientation of the bar and spiral arms at the beginning of the simulations (i.e 4.6 Gyr ago) are defined through the following equations

$$\varphi_b = \varphi_b(0) - \Omega_{bar}t,$$
$$\varphi_s = \varphi_s(0) - \Omega_{sp}t. \qquad (1)$$

Here $\varphi_b(0)$ is the present-day orientation of the bar. We assume that the spiral arms start at the tips of the bar, i.e. $\varphi_s(0) = \varphi_b(0)$ (see Fig. 1). The time, $t = 4.6$ Gyr corresponds to the age of the Sun (Bonanno, Schlattl & Paternò 2002). The initial orientations of the bar and spiral arms are listed in Table 1.

Multiple spiral patterns: we also consider a more realistic Galaxy model with multiple spiral patterns, as suggested by Lépine et al. (2011). In this model, often called the (2 + 2) composite model, two spiral arms have a smaller amplitude and pattern speed than the main structure, which is also composed of two spiral arms. A schematic picture of the composite model is shown in the right-hand panel of Fig. 1. We use the parameters of the composite model suggested by Mishurov & Acharova (2011) and Lépine et al. (2011). These values are listed in Table 2. Here, A_{sp_1} corresponds to a strength of 0.06; that is, the main spiral structure has 6% the strength of the axisymmetric potential. Additionally, the value of Ω_{sp_1} places the co-rotation resonance (CR) of the main spiral structure at the solar radius. The value of Ω_{sp_2} on the other hand, places the CR of the secondary spiral structure at 13.6 kpc. The orientation of the spiral arms at the beginning of the simulation is set according to equation (1), where $\varphi_{0s_1} = 20°$ and $\varphi_{0s_2} = 220°$ are the initial phases
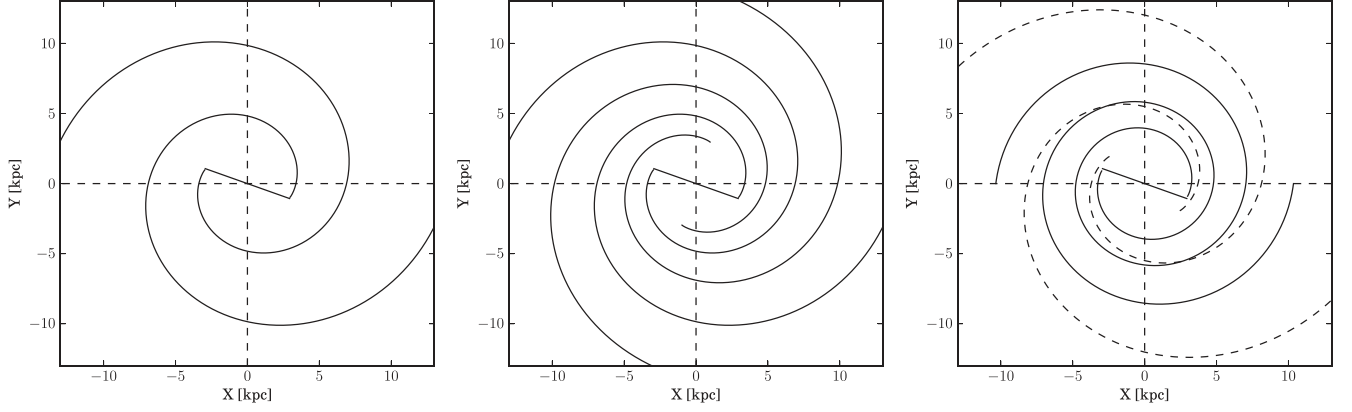
Figure 1. Configurations of the Galactic potential at the present time. Left: galaxy with two spiral arms. Middle: galaxy with four spiral arms. Right: $(2 + 2)$ composite model.

Table 2. Parameters of the composite Galaxy model potential.

Main spiral structure	
Pattern speed (Ω_{sp_1})	26 km s^{-1} kpc^{-1}
Amplitude (A_{sp_1})	650–1300 km^2 s^{-2} kpc^{-1}
Pitch angle (i_1)	$-7°$
Present-day orientation	$20°$
Initial orientation	$171°$
Secondary spiral structure	
Pattern speed (Ω_{sp_2})	15.8 km s^{-1} kpc^{-1}
Amplitude (A_{sp_2})	$0.8A_{sp_1}$
Pitch angle (i_2)	$-14°$
Present-day orientation	$220°$
Initial orientation	$158°$
Bar	
Pattern speed (Ω_{bar})	40 km s^{-1} kpc^{-1}
Semi-major axis (a)	3.12 kpc
Axis ratio (b/a)	0.37
Mass (M_{bar})	9.8×10^9 M$_\odot$
Strength of the bar (ϵ_b)	0.3
Present-day orientation	$20°$
Initial orientation	$1°$

Table 3. Radius (R_c), mass (M_c), number of particles (N) and velocity dispersion (σ_v) adopted for the parental cluster of the Sun.

R_c (pc)	M_c (M$_\odot$)	N	σ_v(km s^{-1})
0.5	510	875	2.91
1	641	1050	2.29
	765	1050	2.27
	1007	1741	2.96
1.5	525	875	1.61
	1067	1740	2.42
2	1023	1741	2.12
	883	1350	2.05
3	804	1500	1.44

of the main and secondary spiral structures respectively. In the composite model we also fixed the parameters of the bar. The corresponding values are listed in Table 2.

2.2 The Sun's birth cluster

2.2.1 Initial conditions

We model the Sun's birth cluster with a spherical density distribution corresponding to a Plummer potential (Plummer 1911). We also assume that the primordial gas was already expelled from the cluster when it starts moving in the Galaxy. The initial mass (M_c) and radius (R_c) of the Sun's birth cluster were set according to Portegies Zwart (2009), who suggested that the Sun was probably born in a cluster with $M_c = 500$–3000 M$_\odot$ and $R_c = 0.5$–3 pc. In Table 3, we show the initial mass and radius of the Sun's birth cluster used in the simulations. From this table, we note that the number of stars belonging to the Sun's birth cluster (N) is around 10^2–10^3 in accordance with previous studies (see e.g. Adams & Laughlin 2001; Adams 2010). In Table 3, we also show the initial velocity dispersion of the Sun's birth cluster (σ_v). This quantity can be computed by

means of the virial theorem. As can be observed, for the initial mass and radius adopted, σ_v is between 1.4 and 2.9 km s^{-1}.

We used a Kroupa initial mass function (IMF; Kroupa 2001) to model the mass distribution of the Sun's birth cluster. The minimum and maximum masses used are 0.08 and 100 M$_\odot$, respectively. In this regime, the IMF is a two-power-law function described by the relation:

$$\psi(m) = \begin{cases} A_1 m^{-1.3} & 0.08 < m \leq 0.5 \text{ M}_\odot, \\ A_2 m^{-2.3} & m > 0.5 \text{ M}_\odot. \end{cases} \quad (2)$$

Here A_1 and A_2 are normalization constants which can be determined by evaluating $\psi(m)$ at the limit masses. We also set the metallicity of the Sun's birth cluster to $Z = 0.02$ ([Fe/H] = 0).

2.2.2 Primordial binary stars

The dynamical evolution of stellar systems is affected by a non-negligible fraction of primordial binaries (see e.g. Tanikawa & Fukushige 2009). Therefore, we also modelled the Sun's birth cluster with different primordial binary fractions in order to observe their effect on the current phase-space distribution of the solar siblings. We varied the primordial binary fraction from zero (only single stars) up to 0.4.

We find that binaries have an effect on the internal evolution of the Sun's birth cluster, in the sense that they tend to halt core collapse. The influence of binaries on the dissolution of siblings throughout the Galactic disc is negligible. We observe that the current spatial distribution of the solar siblings and their astrometric properties are little affected by the primordial binary fraction of the Sun's birth

cluster. Thus, hereafter we focus only on clusters with a primordial binary fraction of zero.

2.2.3 Initial phase-space coordinates

The initial centre of mass coordinates of the Sun's birth cluster $(\boldsymbol{x}_{cm}, \boldsymbol{v}_{cm})$ were computed by integrating the orbit of the Sun backwards in time taking into account the uncertainty in its current Galactocentric position and velocity, using the same methods as Martínez-Barbosa et al. (2015). In these simulations, we ignore the vertical motion of the Sun.

We generate 5000 random positions and velocities from a normal distribution centred at the current Galactocentric phase-space coordinates of the Sun $(\boldsymbol{r}_{\odot}, \boldsymbol{v}_{\odot})$. Thus, the standard deviations (σ) of the normal distribution correspond to the measured uncertainties in these coordinates. We assume that the Sun is currently located at: $\boldsymbol{r}_{\odot} = (-8.5, 0, 0)$ kpc, with $\sigma_{r} = (0.5, 0, 0)$ kpc. In this manner, the uncertainty in $y_{\odot}$ is set to zero given that the Sun is located on the x-axis of the Galactic reference frame (see e.g. Martínez-Barbosa et al. 2015, fig. 1).

The present-day velocity of the Sun is $\boldsymbol{v}_{\odot} = (U_{\odot}, V_{\odot})$; where

$$U_{\odot} \pm \sigma_U = 11.1 \pm 1.2 \text{ km s}^{-1}$$
$$V_{\odot} \pm \sigma_V = (12.4 + V_{LSR}) \pm 2.1 \text{ km s}^{-1}. \quad (3)$$

Here, the vector $(11.1 \pm 1.2, 12.4 \pm 2.1)$ kms^{-1} is the peculiar motion of the Sun (Schönrich, Binney & Dehnen 2010) and V_{LSR} is the velocity of the local standard of rest which depends on the choice of Galactic parameters.

We integrate the orbit of the Sun backwards in time during 4.6 Gyr, for each of the initial conditions in the ensemble. At the end of the integration, we obtain a distribution of possible phase-space coordinates of the Sun at birth $(p(\boldsymbol{x}_b, \boldsymbol{v}_b))$. This procedure was carried out for 125 different Galactic parameters and models, according to the parameter value ranges listed in Tables 1 and 2. We used 111 different combinations of bar and spiral arm parameters for the two- and four-armed spiral models, and 14 different parameters for the composite model.

Once the distribution $p(\boldsymbol{x}_b, \boldsymbol{v}_b)$ is obtained for a given galactic model we use the median of the values of $p(\boldsymbol{x}_b, \boldsymbol{v}_b)$ as the value for $(\boldsymbol{x}_{cm}, \boldsymbol{v}_{cm})$. For the combinations of Galactic parameters used, we found that the median value of $p(\boldsymbol{x}_b, \boldsymbol{v}_b)$ remains in the range of 8.5–9 kpc. This is consistent with Martínez-Barbosa et al. (2015), who found that the Sun hardly migrates in a Galactic potential as the one explained in Section 2.1. We therefore chose to fix $||\boldsymbol{x}_{cm}|| = ||\boldsymbol{x}_b||$ to a value of 9 kpc, with the velocity $\boldsymbol{v}_{cm}$ that corresponds to this value in the function $p(\boldsymbol{x}_b, \boldsymbol{v}_b)$. We note that restricting the birth radius of the Sun for a given Galactic model (fixed bar and spiral arm parameters) limits the possible outcomes for the phase-space distribution of the solar siblings. Different starting radii would lead to different orbits which are affected differently by the bar and spiral arm potentials, which in turn implies different predicted distributions of the solar siblings after 4.6 Gyr. Although we do not account for these differences in outcomes in our simulations, there is still significant spread in the predicted solar sibling distribution caused by the different bar and spiral arm parameters combinations we used (as demonstrated in Section 4).

2.3 Numerical simulations

The various simulation elements described above were to carry out simulations of the evolution of the Sun's birth cluster as it orbits in

the Milky Way potential. We used $9 \times 125 = 1125$ different combinations of birth cluster and Galactic potential parameters, using the parameter choices listed in Tables 1, 2 and 3, in order to study a large variety of possible present-day phase-space distributions of the solar siblings.

We use the HUAYNO code (Pelupessy, Jänes & Portegies Zwart 2012) to compute the gravity among the stars within the cluster. We set the time-step parameter to $\eta = 0.03$. We also use a softening length given by (Aarseth 2003):

$$\epsilon = \frac{4R_{vir}}{N}, \quad (4)$$

where R_{vir} is the initial virial radius of the cluster and N the number of stars.

To calculate the external force due to the Galaxy, we use a sixth-order Rotating BRIDGE (Pelupessy et al. in preparation; Martínez-Barbosa et al. 2015). We set the BRIDGE time-step to $dt = 0.5$ Myr.[1]

The stellar evolution effects were modelled with the population synthesis code SEBA (Portegies Zwart & Verbunt 1996; Toonen, Nelemans & Portegies Zwart 2012). The magnitudes and colours of the stars were subsequently calculated from synthetic spectral energy distributions corresponding to the present-day effective temperature and surface gravity of the solar siblings. In addition, the effects of extinction are accounted for. The simulation of photometry is described further in Section 4.

The various codes used to include the simulation elements above are all coupled through the AMUSE framework (Portegies Zwart et al. 2013). In the simulations, we evolve the Sun's birth cluster during 4.6 Gyr.

3 DISRUPTION OF THE SUN'S BIRTH CLUSTER

As the Sun's birth cluster orbits in the Milky Way potential, the tidal field and the effects of the bar and spiral arms will cause the gradual dissolution of the cluster, its stars spreading out over the Galactic disc. Here we briefly summarize our findings on the cluster dissolution times in our simulations. The results are in line with what is already known about the dynamical evolution of open clusters.

To compute the disruption rate of the Sun's birth cluster, it is necessary to know its tidal radius as a function of time. In its general form, the tidal radius is defined by the following expression (Renaud, Gieles & Boily 2011; Rieder et al. 2013)

$$r_t = \left(\frac{GM_c}{\lambda_{max}}\right)^{1/3}. \quad (5)$$

Here G is the gravitational constant, M_c is the mass of the cluster and λ_{max} is the largest eigenvalue of the tidal tensor $\boldsymbol{T}_{ij}$ which is defined as: $\boldsymbol{T}_{ij} = -\frac{\partial^2 \phi}{\partial x_i \partial x_j}$, with ϕ being the Galactic potential.

We use the method of Baumgardt & Makino (2003) to compute the bound mass of the Sun's birth cluster iteratively. At each time-step, we first assume that all stars are bound and we calculate the tidal radius of the system through equation (5), using the value of $\boldsymbol{T}_{ij}$ at the cluster centre. We use the method of Eisenstein & Hut (1998) to calculate the cluster centre. With this first estimate of r_t, we compute the bound mass, which is the mass of the stars that have a distance from the cluster centre smaller than r_t. We use this bound

---

[1] This set-up in the dynamical codes give a maximum energy error per time-step in the simulations of the order of 10^{-7}.
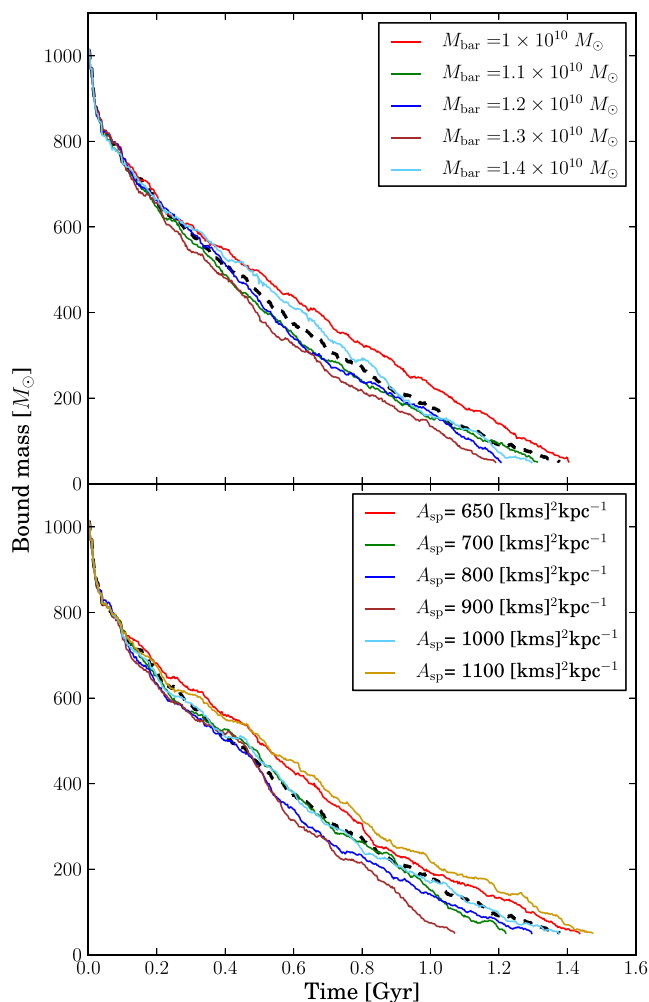
Figure 2. Top: bound mass of the Sun's birth cluster as a function of time for different masses of the central bar of the Galaxy. The dashed black line corresponds to the bound mass of the Sun's birth cluster for a purely axisymmetric Galactic model. Bottom: bound mass of the Sun's birth cluster as a function of time for different amplitudes of the spiral arms. The dashed black line has same meaning as above. Here, the initial mass and radius of the Sun's birth cluster are 1023 $M_{\odot}$ and 2 pc, respectively.

mass and the density centre of the bound particles to recalculate r_t and make a final estimate of the bound mass. We consider the Sun's birth cluster disrupted when 95% of its initial mass is unbound from the cluster.

We studied the effect of the mass of the bar and the spiral arms on the cluster evolution by varying the bar mass or the spiral arm strength, while keeping the other Galactic model parameters fixed. The mass of the bar was varied for a fixed pattern speed of $\Omega_{\rm bar} = 70$ kms^{-1}kpc^{-1}, and with a fixed two-arm spiral with pattern speed $\Omega_{\rm sp} = 20$ kms^{-1}kpc^{-1} and amplitude $A_{\rm sp} = 650$ km s^{-2}kpc^{-1}. The effect of the spiral arm amplitude was studied for a two-arm spiral with pattern speed $\Omega_{\rm sp} = 18$ kms^{-1}kpc^{-1}, and a fixed bar with $M_{\rm bar} = 9.8 \times 10^9$ M$_{\odot}$ and $\Omega_{\rm bar} = 40$ kms^{-1}kpc^{-1}. The resulting evolution of the bound mass of the clusters is shown in Fig. 2, where the top panel shows the effect of varying the bar mass and the bottom panel shows the effect of varying the spiral arm strength. In both cases, we also show the evolution for the case of a purely axisymmetric model of the Galaxy.

From Fig. 2, it is clear that the disruption time of the cluster is not very sensitive to the parameters of the Galactic model. The range of disruption times across all our simulations is 0.5–2.3 Gyr, with additional scatter introduced due to the different perigalactica and eccentricities of the cluster orbits.

4 CURRENT DISTRIBUTION OF SOLAR SIBLINGS IN THE MILKY WAY

If the Sun's birth cluster was completely disrupted in the Galaxy at around 1.8 Gyr, the Sun and its siblings are currently spread out over the Galactic disc, since they have been going around the Galaxy on individual orbits during the last 2.8 Gyr. In Fig. 3, we show four possible distributions of the solar siblings in the Galactic disc. Note that in contrast to the cluster disruption time, the present-day distribution of solar siblings depends strongly on the Galactic parameters, especially on changes in m, $\Omega_{\rm sp}$ and $\Omega_{\rm bar}$. This is because the motion of the solar siblings depends on whether their orbits are affected by the CR$_{\rm sp}$ or by the OLR$_{\rm bar}$. For instance, in panel a of Fig. 3, we observe that there is not much radial migration with respect to the initial position of the Sun's birth cluster ($\bar{R}_{\rm sib} - R_{\rm i} \sim 0.5$ kpc, where $R_{\rm i} = ||\mathbf{x}_{\rm cm}||$). In this example, the Sun and its siblings are not considerably influenced by the CR$_{\rm sp}$ or by the OLR$_{\rm bar}$ during their motion in the Galactic disc. The apocentre and pericentre of the solar siblings is at around 7 and 10 kpc; while the CR$_{\rm sp}$ and OLR$_{\rm bar}$ are located at 11 and 6.7 kpc, respectively. This distribution of solar siblings is similar to the distributions predicted by Portegies Zwart (2009) and Brown et al. (2010).

If the CR$_{\rm sp}$ and the OLR$_{\rm bar}$ are located in the same region where the Sun and its siblings move around the Galaxy, these stars will undergo constant and sudden changes in their angular momentum. As a consequence, the distribution of solar siblings will contain lots of substructures. This effect can be observed in panels b and c of Fig. 3.

When the Sun's birth cluster evolves in a Galaxy containing four spiral arms, the solar siblings undergo considerable radial migration. As a consequence, the current distribution of solar siblings is highly dispersed in galactocentric radius and azimuth, as observed in panel d of Fig. 3. In this Galactic environment, some solar siblings can be located at radial distances of up to 3 kpc different from the radial distance of the Sun to the Galactic Centre.

Mishurov & Acharova (2011) presented the spatial distribution of solar siblings in a Galactic potential with transient spiral structure of different lifetimes. They found that the solar siblings are dispersed all over the disc. Some of these stars can be even located at distances larger than 10 kpc with respect to the Galactic Centre (see figs 9 and 10 in their paper). By comparing these results with the distributions that we obtained for a four-armed spiral structure (panel d, Fig. 3), we infer that the solar siblings would be even more dispersed and located farther from the Sun if the spiral structure of the Milky Way were transient.

Bland-Hawthorn et al. (2010) used stellar diffusion modelling to predict the current distribution of solar siblings in the Galaxy. They used four different approaches, starting from constant and isotropic coefficients to models where they accounted for the impact of churning on the solar siblings. In their approach, the solar siblings are always spread all over the Galactic disc (all azimuths), in a configuration like the one shown in Fig. 3(d). None of their solar siblings distributions show substructures or stellar concentrations in radius and azimuth, as is shown in Fig. 3(a)–(c). Bland-Hawthorn et al. (2010) found that a substantial fraction of solar siblings may be located at galactic longitudes of
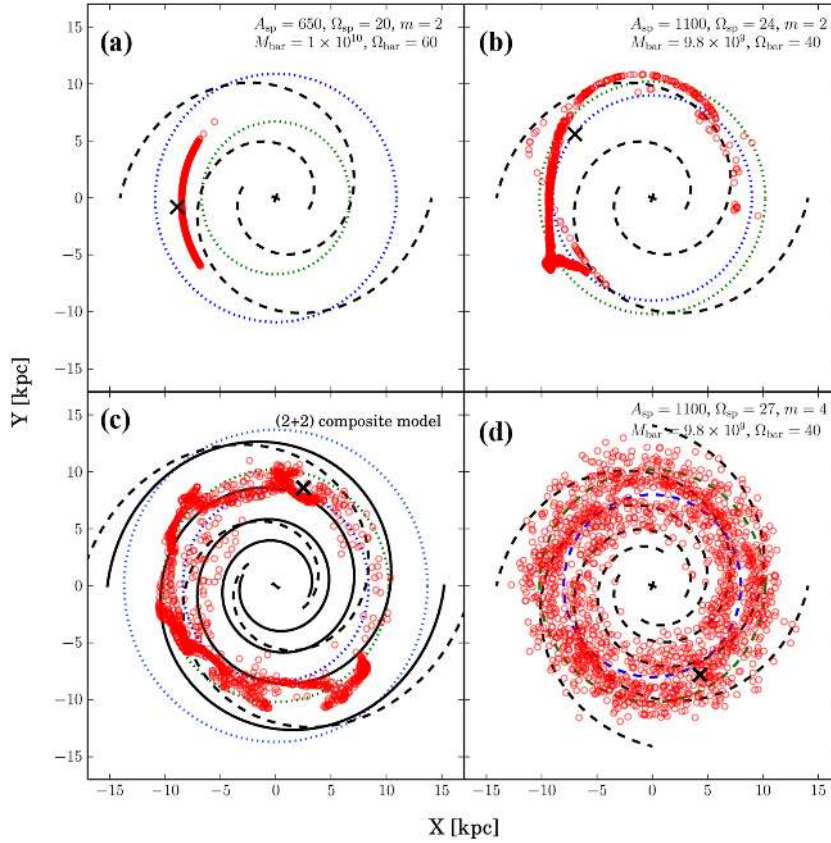
Figure 3. Present-day distribution of solar siblings in the *xy* plane. The point (0, 0) is the centre of the Milky Way. The dashed black lines represent the potential of the spiral arms at present. The dotted blue and green circles correspond to the CR_{sp} and OLR_{bar}, respectively. The black crosses in each panel mark the initial location of the Sun's birth cluster, which is at 9 kpc. Here, the initial mass and radius of the Sun's birth cluster are 1023 $M_\odot$ and 2 parsec, respectively. Top panels: distribution of solar siblings in a Galactic model with two spiral arms. The position of the CR_{sp} and OLR_{bar} are, respectively, (11, 6.7) kpc (a) and (9, 10.2) kpc (b). Bottom panels: (c) Distribution of solar siblings in a (2+2) composite model with $A_{sp1} = 1300$ km^2 s^{-2} kpc^{-1} . The solid and dashed black lines represent the main and secondary spiral structures with co-rotation resonances located at 8.4 and 13.7 kpc, respectively. The OLR_{bar} is at 10.2 kpc. (d) Distribution of solar siblings in a Galactic model with four spiral arms. The CR_{sp} and OLR_{bar} are located at 8 and 10.2 kpc, respectively.

$l = 90°–120°$ or $l = 30°–60°$, depending on the diffusion model employed.

We characterize our predicted present-day distributions of solar siblings by means of their radial and azimuthal dispersion (σ_R and σ_ϕ). These quantities are computed using the Robust Scatter Estimate (RSE; Lindegren et al. 2012). The radial dispersion of the distributions shown in panels a–d in Fig. 3 are $\sigma_R = 0.1, 0.4, 0.9$, and 1.8 kpc, respectively. The angular dispersion of these distributions is: $\sigma_\phi = 0.1\pi, 0.2\pi, 0.4\pi$, and 0.6π rad. Since 0.6π corresponds to the standard deviation of a uniform distribution in azimuth, a highly dispersed distribution (as in panel d of Fig. 3) satisfies $\sigma_R > 0.9$ kpc and $\sigma_\phi > 0.4\pi$ rad.

In Fig. 4, we show the radial and angular dispersion of the current distribution of solar siblings as a function of different Galactic parameters. In the top panel, we varied the parameters of the bar. In the middle and bottom panels, we varied the amplitude and pattern speed of the spiral arms. Note that there is a remarkable increase in σ_R and σ_ϕ when the Galaxy has four spiral arms. In that Galactic potential, 83% of the simulations result in the solar siblings currently being dispersed all over the Galactic disc ($\sigma_R > 0.9$ kpc and $\sigma_\phi > 0.4\pi$ rad). On the contrary, in a Galaxy with two spiral arms (e.g. Fig. 4, top and middle panels), the spatial distribution of solar siblings is more 'clustered' in radius and azimuth. We found that in 84% of these simulations, $\sigma_R < 0.4$ kpc and $\sigma_\phi < 0.2\pi$ rad.
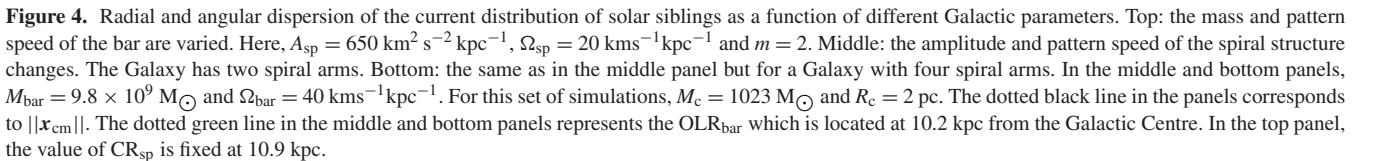
We computed σ_R and σ_ϕ for different initial conditions of the Sun's birth cluster, according to the values presented in Table 3. We found that σ_R and σ_ϕ do not depend on M_c and R_c. The maximum difference in radial and angular dispersion is $\Delta\sigma_{R_{max}} = 0.2$ kpc and $\Delta\sigma_{\phi_{max}} = 0.2\pi$ rad.

The current distribution of solar siblings constrains the number of stars that can be observed near the Sun. For instance, if the solar siblings are 'clustered' in galactocentric radius and azimuth (as shown at the top and middle panels of Fig. 4), the probability of finding a large fraction of solar siblings in the vicinity of the Sun increases. Conversely, in more dispersed solar siblings distributions (e.g. bottom panel, Fig. 4), we expect to find a smaller fraction of solar siblings in the solar vicinity.

We next consider the prospects of identifying solar sibling candidates from the future *Gaia* catalogue data.

5 THE SEARCH FOR THE SOLAR SIBLINGS WITH *Gaia*

The *Gaia* mission will provide an astrometric and photometric survey of more than one billion stars brighter than magnitude $G = 20$ (Lindegren et al. 2008), where G denotes the apparent magnitude in the white light band of used for the astrometric measurements, covering the wavelength range ∼350–1050 nm (see Jordi et al. 2010).

Figure 4. Radial and angular dispersion of the current distribution of solar siblings as a function of different Galactic parameters. Top: the mass and pattern speed of the bar are varied. Here, $A_{sp} = 650$ km^2 s^{-2} kpc^{-1}, $\Omega_{sp} = 20$ kms^{-1}kpc^{-1} and $m = 2$. Middle: the amplitude and pattern speed of the spiral structure changes. The Galaxy has two spiral arms. Bottom: the same as in the middle panel but for a Galaxy with four spiral arms. In the middle and bottom panels, $M_{bar} = 9.8 \times 10^9$ M$_\odot$ and $\Omega_{bar} = 40$ kms^{-1}kpc^{-1}. For this set of simulations, $M_c = 1023$ M$_\odot$ and $R_c = 2$ pc. The dotted black line in the panels corresponds to $||\boldsymbol{x}_{cm}||$. The dotted green line in the middle and bottom panels represents the OLR$_{bar}$ which is located at 10.2 kpc from the Galactic Centre. In the top panel, the value of CR$_{sp}$ is fixed at 10.9 kpc.

Parallaxes (ϖ) and proper motions (μ) will be measured with accuracies ranging from 10 to 30 micro-arcsec (μas) for stars brighter than 15 mag, and from 130 to 600 μas for sources at $G = 20$. For ~100 million stars brighter than $G = 16$, *Gaia* will also measure radial velocities (V_r), with accuracies ranging from 1 to 15 kms^{-1}. *Gaia* will not only revolutionize the current view of the Galaxy but will generate a data set which should in principle allow for a search for solar siblings even far away from the Sun.

In this section, we use our simulations to predict the number of solar siblings that will be seen by *Gaia*, and to study their distribution in the space of parallax, proper motion, and radial velocity with the aim of establishing efficient ways of selecting solar sibling candidates from the *Gaia* catalogue.

5.1 The solar siblings in the *Gaia* catalogue

We first compare the predicted *Gaia* survey of the solar siblings with predictions by Bland-Hawthorn et al. (2010), who considered the

prospects for a survey like GALAH (De Silva et al. 2015) to varying limiting magnitudes. Following Bland-Hawthorn et al. (2010), we broadly distinguish the possible present-day phase configurations for the solar siblings by referring to the cases shown in the panels of Fig. 3 as model a and model b (compact spatial distribution of solar siblings), model c (spatial distribution of solar siblings obtained with the $2 + 2$ composite model) and model d (highly dispersed spatial distribution of solar siblings).

In predicting the observed kinematic properties of the solar siblings, we want to account for the fact that we do not know which of the stars in our simulated clusters is the Sun. The location of the Sun with respect to its siblings will affect the number of siblings that can be observed, especially for clusters that during their dissolution have not spread all over the Galactic disc in azimuth. We therefore proceed as follows. All stars in the simulated cluster located at Galactocentric distances of $R = 8$–9 kpc and with stellar masses around 1 M$_\odot$ are considered possible 'Suns'. The *Gaia* observables (ϖ, μ, V_r) of the siblings are then calculated with respect to each of

these candidate Suns. This results in a set of distributions of siblings over the observables which can be considered collectively in order to account for the uncertain position of the Sun within its dissolved birth cluster.

We used the PYGAIA[2] code to compute the astrometric properties of the solar siblings. Since we are interested in solar siblings that can be observed by *Gaia*, we only include stars for which $G \leq 20$.

The apparent G magnitude is given by the following equation (Jordi et al. [2010])

$$G = -2.5 \log \left(\frac{\int_{\lambda_{min}}^{\lambda_{max}} F(\lambda) 10^{-0.4A_\lambda} S_x(\lambda) d\lambda}{\int_{\lambda_{min}}^{\lambda_{max}} F^{Vega}(\lambda) S_x(\lambda) d\lambda} \right) + G^{Vega} . \qquad (6)$$

Here $F(\lambda)$ and $F^{Vega}(\lambda)$ are the fluxes of a solar sibling and Vega, respectively, as measured above the atmosphere of the Earth (in photons s^{-1} nm^{-1}). We obtain $F(\lambda)$ through the BaSeL library of synthetic spectra (Lejeune, Cuisinier & Buser [1998]), by searching for the stellar spectral energy distribution which best matches the mass (M_s), radius (R_s) and effective temperature (T_{eff}) of a given solar sibling, where the latter quantities are obtained from the stellar evolution part of the simulations. $F^{Vega}(\lambda)$ was obtained in the same way by using the following parameters (Jordi et al. [2010]): $T_{eff} =$ 9550 K, $\log g = 3.95$ dex, [Fe/H] $= -0.5$ dex and $\epsilon_t = 2$ km s^{-1}.

A_λ in equation (6) is the extinction, which is described by

$$A_\lambda = A_V \left(a_\lambda + \frac{b_\lambda}{R_V} \right) , \qquad (7)$$

where A_V is the extinction in the visual (at $\lambda = 550$ nm). The value of A_V within our simulated Galaxy is computed by means of the Drimmel extinction model (Drimmel, Cabrera-Lavers & López-Corredoira [2003]). R_V is the ratio between the extinction and colour excess in the visual band; we use $R_V = 3.1$. a_λ and b_λ are coefficients calculated trough the Cardelli extinction law (Cardelli, Clayton & Mathis [1989]).

The function $S_x(\lambda)$ in equation (6) corresponds to the *Gaia* pass-bands, which depend on the telescope transmission and the CCD quantum efficiency. To compute the stellar magnitude in G, we use the corresponding pass-band described in Jordi et al. ([2010]).

Finally, G^{Vega} is the magnitude zero-point which is fixed through the measurement of the flux of Vega, such that $G^{Vega} = 0.03$ mag.

In Fig. [5] and Table [4], we show the number of solar siblings that might be observed by *Gaia* as a function of their heliocentric distances d and their magnitudes G, where we have averaged over each of the candidate Suns per model. Note that for models a, c and d the largest fraction of solar siblings is located within ~500 pc from the Sun. Yet, the number of solar siblings located at this distance is rather small for some cases. In models c and d for instance, just 18 and 4 solar siblings are at $d \leq 500$ pc on average (see Table [4]). In model a, on the other hand, 145 ± 49 solar siblings might be identified. In model b, the solar siblings are almost uniformly distributed throughout the entire range of d, with more stars at $1.5 \lesssim d \lesssim 3.3$ kpc. A closer look at Fig. [5] (and also at Table [4]) reveals that only in the most 'clustered' spatial distribution of solar siblings (model a), there is a chance to observe tens of solar siblings within 100 pc from the Sun, in accordance with Portegies Zwart ([2009]) and Valtonen et al. ([2015]). In model d, on the contrary, it is not possible to observe substantial numbers of solar siblings near the Sun.

Similar predictions of the observable number of solar siblings were made by Bland-Hawthorn et al. ([2010]) in the context of prepa-
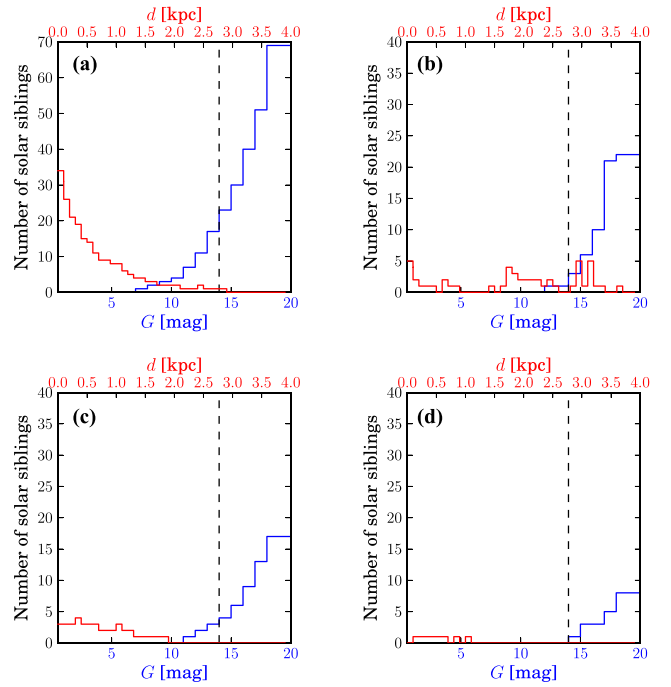
[2] https://pypi.python.org/pypi/PyGaia/

Figure 5. Median number of solar siblings that *Gaia* is predicted to observe, as a function of their heliocentric distances d (red histograms) and G magnitudes (blue histograms). The letters in the left corner correspond to the distributions shown in Fig. [3]. The vertical dotted black lines in each panel represent the limiting magnitude of the GALAH survey, $G \sim 14$ mag.

Table 4. Median and RSE of the number of solar siblings observed at different heliocentric distances and to different limits in G. The last column lists the total number of solar siblings out to the magnitude limit listed. The first column refers to the distributions shown in Fig. [3]. The statistics for a given model were obtained from the distribution of the number of observable solar siblings predicted for each of the candidate Suns.

Model	G (mag)	$d \leq 100$ pc	$d \leq 500$ pc	$d \leq 1$ kpc	total
a	≤ 14	14 ± 5	26 ± 7	30 ± 7	31 ± 7
	≤ 16	22 ± 8	50 ± 16	62 ± 18	72 ± 19
	≤ 18	31 ± 13	95 ± 33	121 ± 39	146 ± 38
	≤ 20	33 ± 14	145 ± 49	199 ± 62	268 ± 57
b	≤ 14	1 ± 0.3	1 ± 0.6	1 ± 0.6	1 ± 0.6
	≤ 16	1 ± 0.9	3 ± 1	3 ± 1	4 ± 1
	≤ 18	3 ± 2	8 ± 4	10 ± 6	19 ± 2
	≤ 20	5 ± 3	14 ± 8	19 ± 11	61 ± 0.3
c	≤ 14	1 ± 1	4 ± 2	5 ± 3	6 ± 3
	≤ 16	1 ± 1	8 ± 4	11 ± 5	15 ± 6
	≤ 18	2 ± 2	13 ± 7	19 ± 11	33 ± 16
	≤ 20	2 ± 2	18 ± 10	37 ± 18	61 ± 31
d	≤ 14	0	0	1 ± 0.7	1 ± 1
	≤ 16	0	1 ± 1	2 ± 1	4 ± 1
	≤ 18	0	2 ± 1	4 ± 1	9 ± 2
	≤ 20	0	4 ± 1	10 ± 2	22 ± 4

rations for chemical tagging surveys, (their table 1). They assumed a larger birth cluster of the Sun (with 2×10^4 stars) with a slightly more massive lower limit on the IMF (0.15 $M_\odot$ versus 0.08 $M_\odot$ in our case).
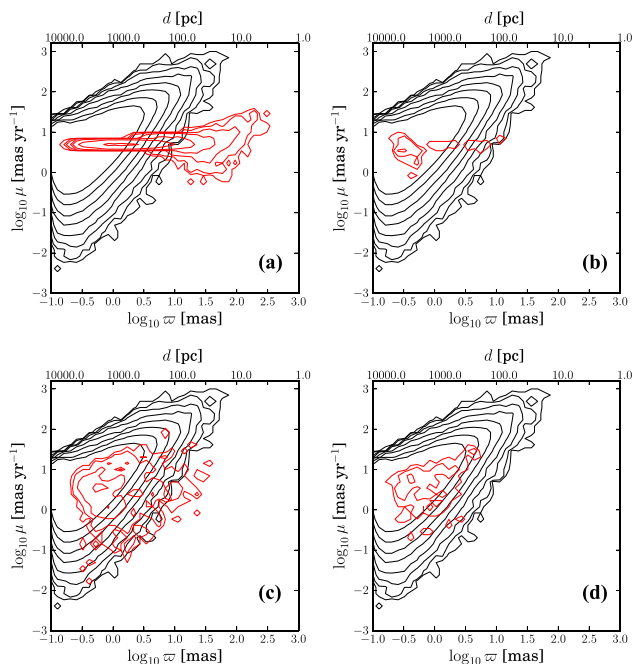
Figure 6. Distribution of solar siblings (red contours) and simulated *Gaia* data for disc stars (black contours) in the proper motion–parallax plane. Each panel corresponds to the distributions shown in Fig. 3. The red and black contours indicate the number of stars in bins of 0.1×0.15 mas^2 yr^{-1}. The contour levels are at 1, 3, 10, 30, 100, 300, 1000 and 3000 stars/bin. In the labels of the top, we also show the heliocentric distance corresponding to each parallax. The proper motion axis represents the total proper motion of the stars.

5.2 Selecting solar sibling candidates from the *Gaia* catalogue

Brown et al. (2010) used their simulated distribution of solar siblings to propose a criterion for the selection of solar sibling candidates on the basis of their observed parallax and proper motion. They basically proposed to select nearby stars with small motions with respect to the Sun. This was motivated by the observation that in that region of the parallax versus proper motion plane, the ratio between the number of siblings and the number of disc stars (in the Hipparcos catalogue) was largest. Given that this contrast between the number of solar siblings and disc stars depends on the details of the Galactic potential (as illustrated in Fig. 3) we revisit the selection criterion proposed by Brown et al. (2010) in order to assess how robust it is against the uncertainties in the present-day distribution of solar siblings. We proceed in a similar way as Brown et al. (2010) and examine the simulated present-day distribution of solar siblings in the space of the astrometric observables (parallax, proper motion, radial velocity), and compare that to the distribution of disc stars. We then search for regions in (ϖ, μ, V_r) where the contrast between solar siblings and disc stars is high.

We illustrate this procedure in Fig. 6. Here, the distribution of solar siblings in the proper motion–parallax plane is represented by the red contours. The black contours correspond to a simulation of field disc stars as measured by *Gaia*. We use the Gaia Universe Model Snapshot (GUMS; Robin et al. 2012) to generate a simulated sample of 2.6×10^7 field disc stars. GUMS represents a synthetic catalogue of stars that simulates what *Gaia* will observe. To select only disc stars, we used only the GUMS stars located in a cylindrical region of radius 8 kpc and height 300 pc (i.e. $|z| \le 150$ pc) centred on to the Sun. The GUMS model includes multiple-star systems. We determine which ones will be resolved by *Gaia* by using a prescrip-

tion employed within the Data Processing and Analysis Consortium (Mignard et al. 2008).[3] In this approach, the angular separation on the sky that *Gaia* can resolve depends on the apparent magnitudes of the stars in the system, with the minimum separation being $\sim$38 mas. For the unresolved cases, a single detection is considered by computing the total integrated magnitude and averaging positions and velocities.

As can be seen in Fig. 6, most of the solar siblings are located well within the overall disc population (at distances over 100 pc) making the selection of sibling candidates on the basis of astrometric and radial velocity data alone very difficult. The only area where a high contrast between the number of siblings and disc stars can be expected is at large parallax and small proper motion values. However, and as expected, this contrast depends strongly on the Galactic potential used in predicting the solar sibling distribution. In order to evaluate the robustness of a selection of sibling candidates in (ϖ, μ, V_r), we must take the uncertainties in their distribution into account and we proceed as follows.

We divide the space ϖ, μ and V_r into discrete (3D) bins and determine for a given simulated solar sibling distribution the number of solar siblings N_{sib} in each bin. We also determine the number of disc stars N_{disc} in each bin and then calculate the number $f_{sib} = N_{sib}/N_{disc}$, which we refer to as the sibling fraction. The idea is that a high value of f_{sib} (say $f_{sib} > 0.5$) suggests that selecting stars from the corresponding (ϖ, μ, V_r) bin in the *Gaia* catalogue should increase the success rate of subsequent searches for solar siblings that examine the astrophysical properties of those stars (age, metallicity, chemical abundance pattern). Alternatively the number f_{sib} can be interpreted as meaning that a star selected from the corresponding bin in (ϖ, μ, V_r) has a probability f_{sib} of being a solar sibling (provided of course that the simulated population of siblings and disc stars is representative of reality).

To account for the uncertainties in the phase-space distribution of siblings, we repeat the above procedure for each of our 1125 simulated solar sibling populations and for each of the 'Suns' within a given population of siblings. This leads to a distribution of values of f_{sib}, $p(f_{sib})$, for each bin in (ϖ, μ, V_r). This distribution thus reflects different Galactic potential parameters, different initial conditions for the Sun's birth cluster, and different possible locations of the Sun within the dispersed sibling population. In Fig. 7, we show the mean value (top panel), the RSE (middle panel) and the survival function [$sf(0.5)$] (bottom panel) of $p(f_{sib})$. The survival function corresponds to the fraction of simulations for which $f_{sib} > 0.5$, which provides a more robust indication of bins in (ϖ, μ, V_r) where a high fraction of solar siblings is likely to be found. Note that the figure shows the statistics for $p(f_{sib})$ marginalized over the coordinate not included in the plot.

The statistics of f_{sib} shown in Fig. 7 show that the proposal by Brown et al. (2010), to search for solar siblings among nearby stars with small motions with respect to the Sun, is robust to the uncertainties in the distribution of the solar siblings due to the uncertain Galactic potential and birth cluster conditions. By examining the (ϖ, μ, V_r) in three dimensions and looking for regions where the mean of $p(f_{sib})$ is above 0.5, we refine the solar sibling candidate selection criterion by Brown et al. (2010) to

$$\varpi \ge 5 \text{ mas};$$
$$4 \le \mu \le 6 \text{ mas yr}^{-1};$$
$$-2 \le V_r \le 0 \text{ km s}^{-1}. \tag{8}$$

---

[3] http://www.cosmos.esa.int/web/gaia/dpac

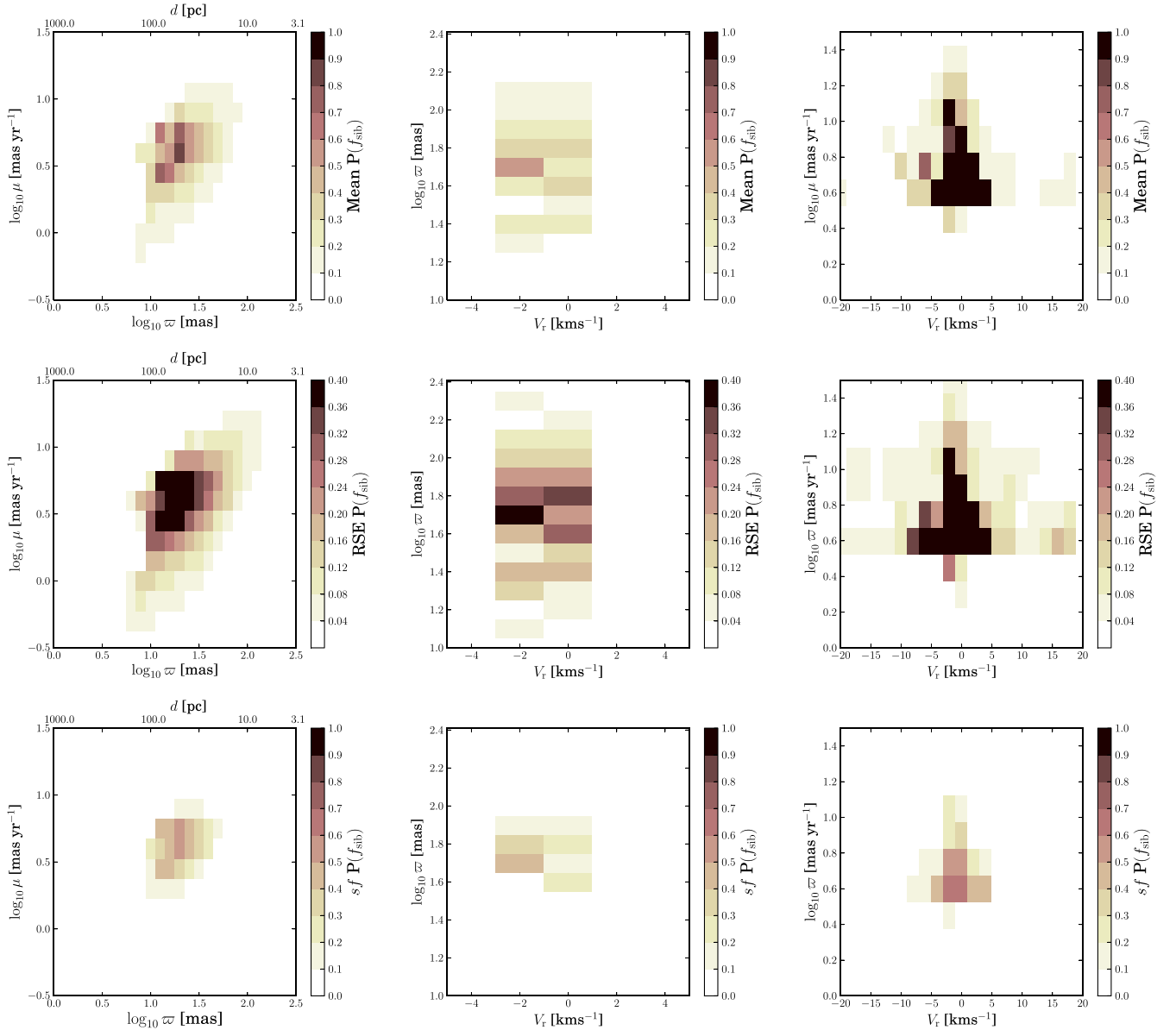**Figure 7.** Mean (top), RSE (middle) and survival function (bottom) of P(f_{sib}) (see the text). We show the projections of such a distribution in the proper motion versus parallax plane (left), in the parallax versus radial velocity plane (middle) and in the proper motion versus radial velocity plane (right). The bin area in each column is (0.1×0.15) mas^2 yr^{-1}, (2×0.15) kms^{-1}mas and (2×0.1) kms^{-1}masyr^{-1}, respectively.

The survival function in this region goes from 0.42 to 0.54. This indicates that despite the uncertainties in the spatial distributions of solar siblings, it is still possible to identify regions in the space of ϖ, μ and V_r where more than a half of the stars might be a solar sibling.

6 DISCUSSION

6.1 Re-evaluation of existing solar sibling candidates

We now use the updated selection criterion from equation (8) to examine the stars that have been proposed in the literature as solar sibling candidates. The results are shown in Table 5. In the first column, we list the names of the solar siblings candidates. From the second to the ninth columns, we show the value and uncertainty of their heliocentric distances, parallaxes, proper motions and radial

velocities, respectively. These values were obtained from the SIMBAD catalogue (Wenger et al. 2000). The tenth column lists mean value of f_{sib} for each star, given its coordinates in the space of ϖ, μ and Vr. The corresponding RSE and the survival fraction for that region of phase space are shown in the 11th and 12th columns, respectively.

Note that the stars HD 147443 and HD 196676 have phase-space coordinates corresponding to sibling fractions of 0.76 ± 0.20 and 0.56 ± 0.38, respectively. Their ages and metallicities are also consistent with those of the Sun (Ramírez et al. 2014). However, given that these stars do not have solar chemical composition (Ramírez et al. 2014), we cannot identify them as solar siblings. This is consistent with the fact that the value of f_{sib} for these stars still allows for a significant fraction of stars that are not solar siblings located in the same region of phase space.

Conversely, Ramírez et al. (2014) found that the stars HD 28676, HD 91320, HD 154747 and HD 162826 have the same age,

Table 5. Current solar siblings candidates. They are sorted by the value of f_{sib}.

Star name (HD no.)	d (pc)	σ_d (pc)	ϖ (mas)	σ_ϖ (mas)	μ (masyr^{-1})	σ_μ (masyr^{-1})	V_r (kms^{-1})	σ_{V_r} (kms^{-1})	f_{sib}	RSE	sf	Ref.[a]
147443	92.0	8.38	10.87	0.99	5.26	0.69	−2.1	7.1	0.76	0.20	0.47	Br10
196676	74.4	2.77	13.44	0.5	5.06	0.54	−0.79	0.1	0.56	0.38	0.42	Br10
192324	67.11	4.82	14.9	1.07	6.36	2.01	−4.4	0.4	0.02	0.01	0.01	Br10
46301	107.64	6.6	9.29	0.57	5.85	0.71	−6.7	0.7	0.01	0.005	0.01	Ba12
162826	33.6	0.41	29.76	0.36	20.14	0.38	1.88	0.0063	0.003	0.001	$\sim 10^{-4}$	Bo11
26690	36.34	0.77	27.52	0.58	3.62	0.58	2.4	1.9	0.003	0.001	$\sim 10^{-4}$	Ba12
207164	76.1	3.82	13.14	0.66	3.06	0.7	−7.0	0.3	0.001	0.0005	$\sim 10^{-4}$	Ba12
35317	55.71	2.39	17.95	0.77	6.08	0.51	15.0	0.1	$\sim 10^{-4}$	$\sim 10^{-4}$	$\sim 10^{-4}$	Ba12
175740	81.97	1.75	12.2	0.26	2.95	0.26	−9.18	0.25	$\sim 10^{-4}$	$\sim 10^{-4}$	$\sim 10^{-4}$	Br10+Ba12
199881	72.2	3.65	13.85	0.7	2.64	0.8	−15.7	0.3	$\sim 10^{-4}$	$\sim 10^{-4}$	$\sim 10^{-4}$	Ba12
101197	82.99	6.82	12.05	0.99	5.66	0.62	7.5	0.3	$\sim 10^{-4}$	$\sim 10^{-4}$	$\sim 10^{-4}$	Ba12
105678	74.02	1.7	13.51	0.31	5.82	0.26	−17.4	0.5	$\sim 10^{-4}$	$\sim 10^{-4}$	$\sim 10^{-4}$	Ba12
219828	72.31	3.87	13.83	0.74	5.86	0.77	−24.14	0.17	$\sim 10^{-4}$	$\sim 10^{-4}$	$\sim 10^{-4}$	Ba12
28676	38.7	0.88	25.84	0.59	4.47	0.73	6.71	0.09	$\sim 10^{-4}$	$\sim 10^{-4}$	$\sim 10^{-4}$	Br10+Ba12
52242	68.17	2.74	14.67	0.59	5.07	0.64	31.3	0.9	$\sim 10^{-4}$	$\sim 10^{-4}$	$\sim 10^{-4}$	Ba12
95915	66.62	2.13	15.01	0.48	5.09	0.53	16.9	0.3	$\sim 10^{-4}$	$\sim 10^{-4}$	$\sim 10^{-4}$	Ba12
105000	71.07	2.98	14.07	0.59	4.73	0.75	−14.8	1.5	$\sim 10^{-4}$	$\sim 10^{-4}$	$\sim 10^{-4}$	Ba12
148317	79.62	3.49	12.56	0.55	3.45	0.69	−37.6	0.4	$\sim 10^{-4}$	$\sim 10^{-4}$	$\sim 10^{-4}$	Ba12
44821	29.33	0.53	34.1	0.62	5.0	0.44	18.3	0.76	$\sim 10^{-4}$	$\sim 10^{-4}$	$\sim 10^{-4}$	Br10+Ba12
68814	80.45	7.57	12.43	1.17	3.65	1.03	34.5	0.3	$\sim 10^{-4}$	$\sim 10^{-4}$	$\sim 10^{-4}$	Liu15
7735	85.69	8.81	11.67	1.2	3.5	1.18	21.7	1.4	$\sim 10^{-4}$	$\sim 10^{-4}$	$\sim 10^{-4}$	Ba12
100382	93.98	3.0	10.64	0.34	4.89	0.35	−10.9	0.4	$\sim 10^{-4}$	$\sim 10^{-4}$	$\sim 10^{-4}$	Br10
199951	70.22	1.28	14.24	0.26	1.78	0.21	17.6	0.8	$\sim 10^{-4}$	$\sim 10^{-4}$	$\sim 10^{-4}$	Ba12
168769	50.18	3.7	19.93	1.47	2.14	1.33	26.4	0.2	$\sim 10^{-4}$	$\sim 10^{-4}$	$\sim 10^{-4}$	Br10
46100	55.46	2.61	18.03	0.85	9.35	0.94	21.3	0.3	$\sim 10^{-4}$	$\sim 10^{-4}$	$\sim 10^{-4}$	Ba12
83423	72.1	4.94	13.87	0.95	7.96	1.2	−7.3	3.4	$\sim 10^{-4}$	$\sim 10^{-4}$	$\sim 10^{-4}$	Bo11+Ba12
91320	90.5	6.88	11.05	0.84	5.18	0.63	17.5	0.4	$\sim 10^{-4}$	$\sim 10^{-4}$	$\sim 10^{-4}$	Br10
102928	91.41	4.18	10.94	0.5	0.63	0.34	14.12	0.06	$\sim 10^{-4}$	$\sim 10^{-4}$	$\sim 10^{-4}$	Br10
168442	19.56	0.62	51.12	1.63	2.3	1.56	−13.8	0.3	$\sim 10^{-4}$	$\sim 10^{-4}$	$\sim 10^{-4}$	Br10
154747	97.85	8.9	10.22	0.93	8.58	0.78	−14.9	0.3	$\sim 10^{-4}$	$\sim 10^{-4}$	$\sim 10^{-4}$	Ba12
183140	71.84	6.61	13.92	1.28	13.97	0.91	−28.8	0.4	$\sim 10^{-4}$	$\sim 10^{-4}$	$\sim 10^{-4}$	Ba12

[a]Br10 = Brown et al. (2010); Bo11 = Bobylev et al. (2011); Ba12 = Batista & Fernandes (2012); Liu14 = Liu et al. (2015)

metallicity and chemical composition as the Sun, within the observational errors. However, according to the numbers in Table 5, these stars have a low probability of being solar siblings. This also holds for the star HD 68814, which is chemically homogeneous with the Sun (Liu et al. 2015) but is located in a phase-space region where $f_{sib} \sim 10^{-4}$. This discrepancy may be due to the limitations in our simulations, which may lead to underestimates of f_{sib} (see Section 6.2) or may be attributed to the observation that there is chemical abundance overlap between different clusters (Blanco-Cuaresma et al. 2015), which implies the presence of stars that look like solar siblings even if their phase-space properties are very different.

From the small number of stars examined as potential solar siblings, it is not possible to draw further conclusions. For more progress on this issue the results of *Gaia* and the complementary abundance surveys, such as GALAH, will have to be awaited.

6.2 Applicability of the sibling selection criteria

We have shown in this study that despite uncertainties in the Galactic potential parameters and solar birth cluster initial conditions, it is possible to identify a region in the space of parallaxes, proper motion, and radial velocities which is robustly predicted to contain a high fraction of solar siblings with respect to disc stars. However, the selection criterion shown in equation (8) is only valid for the cluster initial conditions and Galaxy models considered here. Changes in the mass and size of the Sun's birth cluster or in the modelling of

the Milky Way, might alter the region in phase space where it is more likely to identify solar siblings. For instance, massive clusters (with 10^4 stars) evolving in the Galactic potential described in Section 2.1 might have lifetimes of around 20 Gyr (Gieles et al. 2007). Thus, after 4.6 Gyr of evolution, most of the solar siblings would still be bound to the cluster, showing a clumped distribution in the phase space for most of the Galactic parameters. Conversely, small open clusters (as those described in Section 2.2) only survive a few Myr in a Galaxy model containing transient spiral structure and giant molecular clouds (see e.g. Gieles et al. 2006, 2007; Lamers & Gieles 2006; Kruijssen et al. 2011). In such a more realistic potential the solar siblings would be more dispersed in both radius and azimuth, completely mixed with other disc stars, which would (much) lower the mean value of f_{sib} in any given region of (ϖ, μ, V_r). Another limitation is that we do not consider the vertical motion of the Sun and the vertical force of the bar and spiral arms in the cluster simulations. Although the solar siblings are stars that move within the Galactic disc, the mean value of f_{sib} might change when considering a 3D potential for the Galaxy. For the types of solar birth clusters studied in this work, the results thus strongly support the need for chemical abundance surveys to attempt to identify the Sun's siblings (and other disrupted clusters).

One could consider making more sophisticated phase-space searches for the solar siblings by making use of conserved quantities (energy, angular momentum). However, if open clusters contribute a significant fraction of the stars to the Galactic disc (and all stars existing on somewhat similar orbits) it is not obvious that disrupted

open clusters would stand out in integrals of motion spaces. Our simple selection criterion also has the advantage of being defined entirely in the space of observables where the properties of the errors are well understood.

7 SUMMARY

We used numerical simulations to study the evolution and disruption of the Sun's birth cluster in the Milky Way. In the simulations, we include the gravitational force among the stars in the cluster and the stellar evolution effects on the cluster population. We also include the external tidal field of the Galaxy, which was modelled as an analytical potential containing a bar and spiral arms. We used two Galactic models: one in which the Galaxy has two or four spiral arms and a $(2 + 2)$ composite model in which two spiral arms have smaller strength and pattern speed than the other two arms. The aim of this study is to predict the present-day phase-space distribution of the solar siblings (as observed in astrometry and radial velocities) and to understand how *Gaia* data might be used to pre-select solar siblings candidates for follow-up chemical abundance studies.

We found that the dissolution time-scale of the Sun's birth cluster is insensitive to the details of the Galactic model, in particular to the parameters of the bar and spiral arms. For the set of simulations carried out in this study, the Sun's birth cluster is completely disrupted in a time-scale of 0.5–2.3 Gyr, where the differences are due to different eccentricities and perigalactica of the cluster orbits.

After the dissolution of the Sun's birth cluster, the solar siblings move independently within the potential of the Galaxy. Depending on the Galactic parameters, the solar siblings may currently be more or less dispersed in Galactic radius and azimuth. If the orbits of the solar siblings are not influenced by the CR_{sp} or by the OLR_{bar}, the present-day distribution of the solar siblings is such that most of these stars are in the close vicinity of the Sun. Conversely, if the orbits of the solar siblings are influenced by these two resonances, the current spatial distribution of the siblings is more dispersed in radius and azimuth, with substructures in some regions of the Galactic disc [this is also observed in the $(2 + 2)$ composite model]. In Galaxy models with four spiral arms, the solar siblings are spread all over the Galactic disc.

We predicted the *Gaia* observations (astrometry and radial velocities) of solar siblings brighter than $G = 20$ mag. We use the GUMS simulation (Robin et al. 2012) to generate a large sample of stars which mimic the disc stars that *Gaia* will observe. With this information, we computed the sibling fraction $f_{sib} = N_{sib}/N_{dism}$, which can be interpreted as the probability of finding solar siblings in a certain region of the space of ϖ, μ and V_r. Regions in this phase space where $f_{sib} > 0.5$ indicate that a large fraction of stars located there might be solar siblings. Thus, exploring those regions would increase the success rate in finding solar siblings candidates in the future. We found that $f_{sib} > 0.5$ when $\varpi \geq 5$ mas, $4 \leq \mu \leq 6$ mas yr^{-1}, and $-2 \leq V_r \leq 0$ km s^{-1}. This result is very similar to that by Brown et al. (2010) but is now obtained for a large fraction of simulations covering a broad range of Galactic parameters and initial conditions for the Sun's birth cluster.

However, this selection criterion is only valid under the assumptions made in this study. Introducing more realism into the simulations (transient spiral arms, molecular clouds) would lower f_{sib} and make the pre-selection of solar siblings on the basis of distance and kinematic data very inefficient (unless the Sun's birth cluster was originally much more massive). This reinforces the conclusion already reached by Bland-Hawthorn et al. (2010) that large-scale surveys are needed which are aimed at precisely determining the as-

trophysical properties of stars, in particular their ages and chemical abundances, if we want to identify the solar family.

REFERENCES

Aarseth S. J., 2003, Gravitational N-Body Simulations. Cambridge Univ. Press, Cambridge
Adams F. C., 2010, ARA&A, 48, 47
Adams F. C., Laughlin G., 2001, Icarus, 150, 151
Allen C., Santillán A., 1991, Rev. Mex. Astron. Astrofis., 22, 255
Batista S. F. A., Fernandes J., 2012, New Astron., 17, 514
Batista S. F. A., Adibekyan V. Z., Sousa S. G., Santos N. C., Delgado Mena E., Hakobyan A. A., 2014, A&A, 564, A43
Baumgardt H., Makino J., 2003, MNRAS, 340, 227
Berentzen I., Athanassoula E., 2012, MNRAS, 419, 3244
Blanco-Cuaresma S. et al., 2015, A&A, 577, A47
Bland-Hawthorn J., Krumholz M. R., Freeman K., 2010, ApJ, 713, 166
Bobylev V. V., Bajkova A. T., Mylläri A., Valtonen M., 2011, Astron. Lett., 37, 550
Bonanno A., Schlattl H., Paternò L., 2002, A&A, 390, 1115
Brown A. G. A., Portegies Zwart S. F., Bean J., 2010, MNRAS, 407, 458
Cardelli J. A., Clayton G. C., Mathis J. S., 1989, ApJ, 345, 245
De Silva G. M. et al., 2015, MNRAS, 449, 2604
Drimmel R., Cabrera-Lavers A., López-Corredoira M., 2003, A&A, 409, 205
Dukes D., Krumholz M. R., 2012, ApJ, 754, 56
Eisenstein D. J., Hut P., 1998, ApJ, 498, 137
Ferrers N. M., 1877, Pure Appl. Math., 14, 1
Fujii M. S., Baba J., 2012, MNRAS, 427, L16
Gieles M., Portegies Zwart S. F., Baumgardt H., Athanassoula E., Lamers H. J. G. L. M., Sipior M., Leenaarts J., 2006, MNRAS, 371, 793
Gieles M., Athanassoula E., Portegies Zwart S. F., 2007, MNRAS, 376, 809
Gieles M., Heggie D. C., Zhao H., 2011, MNRAS, 413, 2509
Jílková L., Carraro G., Jungwiert B., Minchev I., 2012, A&A, 541, A64
Jordi C. et al., 2010, A&A, 523, A48
Kroupa P., 2001, MNRAS, 322, 231
Kruijssen J. M. D., Pelupessy F. I., Lamers H. J. G. L. M., Portegies Zwart S. F., Icke V., 2011, MNRAS, 414, 1339
Lada C. J., Lada E. A., 2003, ARA&A, 41, 57
Lamers H. J. G. L. M., Gieles M., 2006, A&A, 455, L17
Lee Y.-W. et al., 2013, ApJ, 778, L13
Lejeune T., Cuisinier F., Buser R., 1998, A&AS, 130, 65
Lépine J. R. D. et al., 2011, MNRAS, 417, 698
Lin C. C., Yuan C., Shu F. H., 1969, ApJ, 155, 721
Lindegren L. et al., 2008, in Jin W. J., Platais I., Perryman M. A. C., eds, Proc. IAU Symp. 248, A Giant Step: From Milli- to Micro-arcsecond Astrometry. Kluwer, Dordrecht, p. 217
Lindegren L., Lammers U., Hobbs D., O'Mullane W., Bastian U., Hernández J., 2012, A&A, 538, A78
Liu C., Ruchti G., Feltzing S., Martínez-Barbosa C. A., Bensby T., Brown A. G. A., Portegies Zwart S. F., 2015, A&A, 575, A51
McMillan P. J., 2011, MNRAS, 414, 2446
Madrid J. P., Hurley J. R., Sippel A. C., 2012, ApJ, 756, 167
Madrid J. P., Hurley J. R., Martig M., 2014, ApJ, 784, 95
Martínez-Barbosa C. A., Brown A. G. A., Portegies Zwart S., 2015, MNRAS, 446, 823

Mignard F. et al., 2008, in Jin W. J., Platais I., Perryman M. A. C., eds, Proc. IAU Symp. 248, A Giant Step: From Milli- to Micro-arcsecond Astrometry. Kluwer, Dordrecht, p. 224

Minchev I., Famaey B., 2010, ApJ, 722, 112

Mishurov Y. N., Acharova I. A., 2011, MNRAS, 412, 1771

Miyamoto M., Nagai R., 1975, PASJ, 27, 533

Pelupessy F. I., Jänes J., Portegies Zwart S., 2012, New Astron., 17, 711

Pichardo B., Martos M., Moreno E., 2004, ApJ, 609, 144

Pichardo B., Moreno E., Allen C., Bedin L. R., Bellini A., Pasquini L., 2012, AJ, 143, 73

Plummer H. C., 1911, MNRAS, 71, 460

Portegies Zwart S. F., 2009, ApJ, 696, L13

Portegies Zwart S. F., Jílková L., 2015, MNRAS, 451, 144

Portegies Zwart S. F., Verbunt F., 1996, A&A, 309, 179

Portegies Zwart S., McMillan S. L. W., van Elteren E., Pelupessy I., de Vries N., 2013, Comput. Phys. Commun., 183, 456

Ramírez I. et al., 2014, ApJ, 787, 154

Reid M. J. et al., 2014, ApJ, 783, 130

Renaud F., Gieles M., Boily C. M., 2011, MNRAS, 418, 759

Rieder S., Ishiyama T., Langelaan P., Makino J., McMillan S. L. W., Portegies Zwart S., 2013, MNRAS, 436, 3695

Robin A. C. et al., 2012, A&A, 543, A100

Romero-Gómez M., Athanassoula E., Antoja T., Figueras F., 2011, MNRAS, 418, 1176

Schönrich R., Binney J., Dehnen W., 2010, MNRAS, 403, 1829

Takahashi K., Portegies Zwart S. F., 2000, ApJ, 535, 759

Tanikawa A., Fukushige T., 2009, PASJ, 61, 721

Toonen S., Nelemans G., Portegies Zwart S., 2012, A&A, 546, A70

Valtonen M., Bajkova A. T., Bobylev V. V., Mylläri A., 2015, Celest. Mech. Dyn. Astron., 121, 107

Webb J. J., Sills A., Harris W. E., Hurley J. R., 2014, MNRAS, 445, 1048

Wenger M. et al., 2000, A&AS, 143, 9

This paper has been typeset from a TEX/LATEX file prepared by the author.